Quasi-Static Design Technique for mm-Wave Micromachined Filters with Lumped Elements and Series Stubs

Thomas M. Weller, *Member, IEEE,* Katherine J. Herrick, and Linda P. B. Katehi, *Fellow, IEEE*

***Abstract*— This paper describes micromachined, membrane-supported low-pass and bandpass filters which are suitable for microwave and millimeter-wave (mm-wave) application. The designs are realized in coplanar-waveguide (CPW) form using short- and open-end series stubs with integrated metal–insulator–metal (MIM) capacitors, and are compact in lateral and longitudinal dimensions. A computationally efficient analysis has been developed for the design and characterization of the filters. The technique is based on a quasi-static coupled-line (CL) treatment of the series stubs, and uses normal mode impedance parameters, which are calculated with the spectral-domain approach (SDA). Due to the broad TEM-bandwidth of the membrane-supported transmission lines, the method can accurately predict filter responses well into the rejection band. To demonstrate the above claims, the measured and simulated S-parameters of a 0.3 mm $\times$ 2.2 mm low-pass filter with a cutoff frequency at 17 GHz, and a second passband at 115 GHz, are presented. The new approach is also used in the design of bandpass filters which exhibit 1.5–2-dB insertion loss and bandwidths around 10%.**

***Index Terms*— Coplanar waveguide, coupled lines, filters, micromachining, millimeter wave.**

I. Introduction

MICROMACHINED transmission lines supported by thin dielectric membranes have proven to be high-performance alternatives for millimeter-wave (mm-wave) applications. A membrane-supported microstrip has been used to develop lumped components such as spiral inductors with low parasitic capacitance, and low-loss, coupled-line (CL) bandpass filters at W-band [1], [2]. The microshield geometry (Fig. 1) is a membrane-supported coplanar waveguide (CPW) that has been demonstrated at frequencies from Ka-band to 250 GHz [3]–[5]. The strengths of these monolithic architectures primarily derive from the homogeneous air dielectric, and include broad TEM bandwidth, minimal dispersion, and zero dielectric loss.

Although the membrane line offers excellent performance, certain characteristics of it present potential difficulties for component design. The two primary challenges are realizing physically compact structures and achieving a low characteristic impedance. Since the effective dielectric constant is approximately equal to one, the line lengths on a membrane are nearly 2.5 times longer than equivalent lines on silicon or GaAs. Distributed circuits, such as filters, thus require greater amounts of surface area when realized in microshield or membrane-supported microstrip. The low dielectric constant also makes it more difficult to achieve a low characteristic impedance. This effect can significantly impact the topology of circuits such as low-pass filters, which are commonly designed using the stepped-impedance approach.

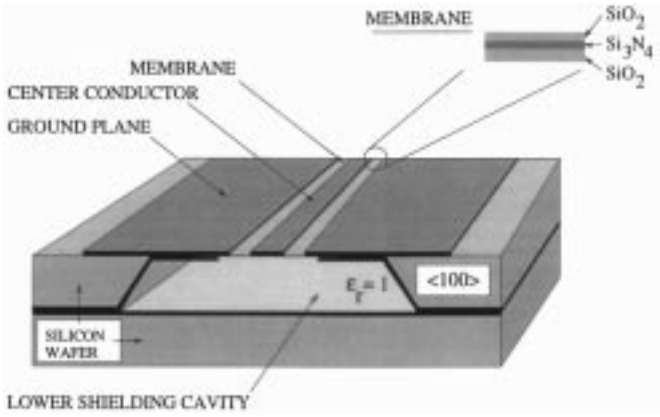

Fig. 1. Membrane-supported microshield transmission line.

In order to address these issues, a new architecture for mm-wave filters has been developed and its use in the design of microshield low-pass and bandpass filters is presented herein. The topology used for the low-pass filters is a combination of series short-end stubs with integrated metal–insulator–metal (MIM) overlay capacitors (Fig. 2). A similar geometry suitable for bandpass filters uses an open-end stub in place of the shorted stub (Fig. 3). The results presented in this paper demonstrate the advantages of combining lumped capacitors with semidistributed elements to achieve low-loss, broad-band performance, and small size at mm-wave frequencies. The technique is not limited to use with micromachined transmission-line geometries, and can potentially be applied to realize alternative circuit functions by choosing different stub configurations.

The first part of the paper will outline a quasi-static analysis that is used to characterize individual resonator elements. A design procedure for low-pass filters, based on this analysis, is then presented and verified using measured filter data up to 117 GHz. Finally, measured and simulated data are compared for bandpass filter implementations.

Manuscript received July 5, 1996; revised February 28, 1997.

T. M. Weller is with the Microwave and Wireless Laboratory, University of South Florida, Tampa, FL 33620 USA.

K. J. Herrick and L. P. B. Katehi are with the Radiation Laboratory, University of Michigan, Ann Arbor, MI 48109 USA.

Publisher Item Identifier S 0018-9480(97)03916-1.

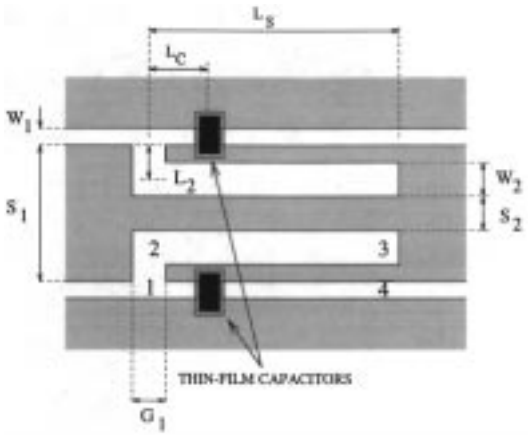

Fig. 2. Series short-end stub with MIM capacitors. The numbers 1–4 indicate the port assignments used in the CL analysis.

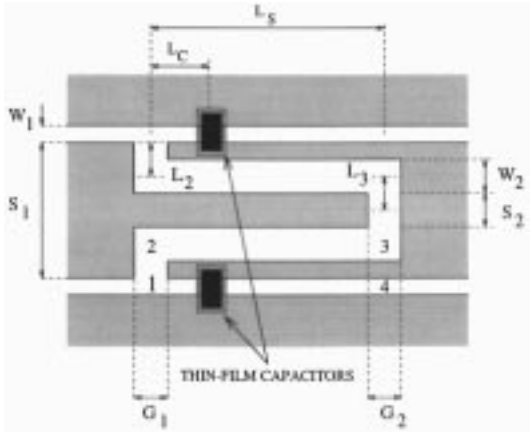

Fig. 3. Series open-end stub with MIM capacitors. The numbers 1–4 indicate the port assignments used in the CL analysis.

II. Quasi-Static Analysis

The theory applied herein is based on a variation of the quasi-static, CL analysis presented in [6]. Getsinger [7] originally proposed that the open- and short-end series stubs can be treated as two pair of asymmetric coupled slots, with magnetic wall symmetry down the center-line. Consequently, two slots on a given side can be characterized using a four-port analysis. This is a computationally efficient approach which is accurate over the bandwidth of TEM operation and, as will be shown, allows the overlay capacitors to be easily incorporated into the model.

In order to calculate the slot impedance parameters which are required in the CL analysis, the spectral-domain approach (SDA) [8] was employed. The SDA was chosen for this step because it is relatively easy to implement and is flexible in terms of the geometries for which it can be used. It is also important to note that, due to its broad-band TEM nature, the microshield line has slot characteristics which are essentially independent of frequency. As a result, the full-wave (FW) SDA technique only needs to be executed at one midband frequency point for any given stub geometry.

Previously published works concerning the characterization of the CPW series stubs include FW [3], [9], [10], quasi-static [11], and experimental techniques [12], [13]. As long as the circuit dimensions are appropriately chosen, the high degree of accuracy afforded by the FW methods has been found to be unnecessary for this analysis. The computational requirements and complexity of modeling stubs with integrated MIM capacitors makes this approach even less attractive. A quasi-static analysis of series stubs that was outlined in [11] is similar to that used here, but the associated filter-design approach was not intended to accommodate lumped capacitors. The concepts applied here also find precedence in previous applications of the SDA for CL characterization (e.g., [14]).

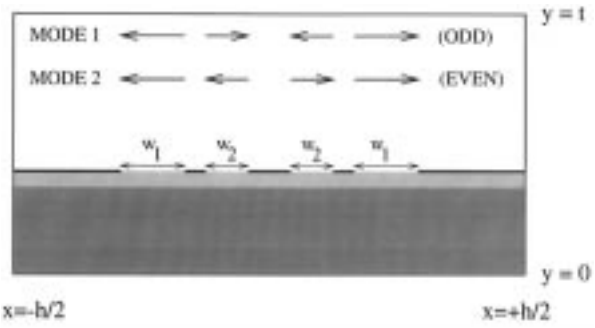

Fig. 4. Cross section of a shielded CPW line with three center conductors. The direction of the slot electric fields (x-component) for two normal modes is shown at the top of the figure.

A. Spectral-Domain Analysis

The spectral-domain analysis is used for the calculation of the propagation constants, slot impedances, and excitation voltages for the normal modes of the three center-conductor CPW geometry shown in Fig. 4. This figure is a cross-sectional view of either the open- or short-end series stub with two substrate layers (e.g., membrane and air), enclosed in a shielding cavity. In typical fashion, the partially shielded configuration is approximated by sufficiently displacing both the upperwalls and sidewalls.

Assuming that a CPW-type excitation is used and that the circuit possesses transverse symmetry, the slot fields for the propagating modes must also be laterally symmetric. As a result, the two possible modes are those depicted in Fig. 4. This geometry requires an independent set of expansion functions for the inner and outer slot pairs ($i = 1, 2$), which are of the form

$$E_{x,i} = \sum_{m=1}^{M} c_{i,m} E_{xm,i}$$
$$E_{z,i} = \sum_{n=1}^{N} d_{i,n} E_{zn,i}. \tag{1}$$

The basis functions $E_{xm,i}$ and $E_{zn,i}$ are comprised of even and odd sinusoidal functions, defined according to [8].

The propagation constants for the normal modes are found by solving for the roots of the determinant of the SDA admittance matrix. This matrix is generated by applying Galerkin's technique to the linear system, which relates the electric fields and currents over the cross section, using a spectral-domain Green's function. For each mode and each slot, the

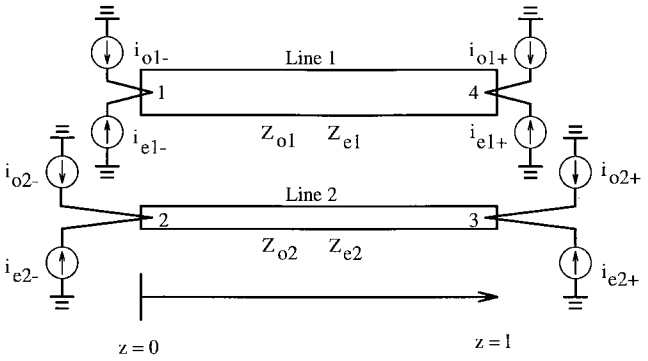

Fig. 5. Physical configuration of two asymmetric coupled lines and the even- and odd-mode current excitations.

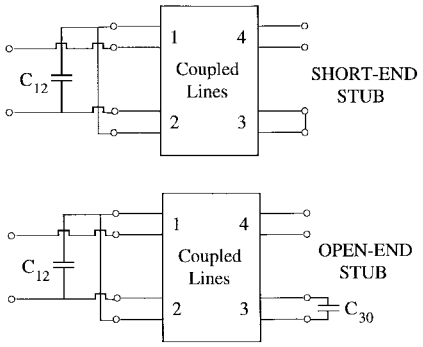

Fig. 6. Modified four-port CL circuits used to model short- and open-end series stubs.

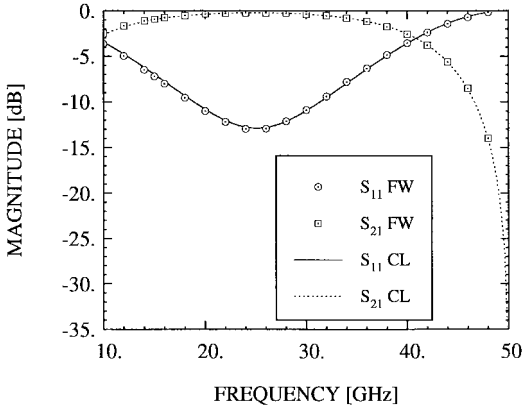

Fig. 7. Comparison between the results from a FW analysis and the CL technique. The circuit is a CPW GaAs open-end series stub with the following dimensions: $L_s = 1100$, $S_1 = 120$, $S_2 = 40$, $W_1 = 85$, $W_2 = 20$, $G_1 = 40$, $G_2 = 40\mu$m.

characteristic impedance and voltage can then be evaluated. Details of this analysis can be found in [15].

B. Coupled-Line Analysis

With the slot characteristics known, coupled-transmission-line theory [6] is used to generate a four-port impedance matrix. Due to symmetry, only half of the stub geometry needs to be considered, and the two slots on a given side can be represented by the CL configuration given in Fig. 5. In this figure, the $-$ and $+$ in the subscripts denote the left and right side, respectively. In reference to phase relationships, the two modes are denoted as odd and even, corresponding to modes 1 and 2, respectively, in Fig. 4.

Since the slots are asymmetric, the current excitations shown in Fig. 5 must differ in magnitude. With symmetric lines, the sources are related as follows:

$$\begin{aligned} i_{e1\pm} &= i_{e2\pm} \\ i_{o1\pm} &= -i_{o2\pm}. \end{aligned} \tag{2}$$

In the asymmetric case, the relationships become

$$\begin{aligned} \alpha &= \frac{Z_{e1}V_{e2}}{Z_{e2}V_{e1}} \\ \kappa &= -\frac{Z_{o1}V_{o2}}{Z_{o2}V_{o1}} \\ i_{e2\pm} &= \alpha i_{e1\pm} \quad \text{even mode} \\ i_{o2\pm} &= -\kappa i_{o1\pm} \quad \text{odd mode} \end{aligned} \tag{3}$$

where the voltages and impedances calculated from the spectral-domain analysis are used. The equations shown in (3) are derived by considering the current–voltage expressions for either normal mode on an infinite line, $V_1 = Z_1 i_1$ and $V_2 = Z_2 i_2$. These equations are used to express the ratio of i_1/i_2 which, in general, is not equal to ± 1. In [16], the equivalents of α and κ are defined in terms of the self- and mutual-impedances of the CL system.

C. Series-Stub Characterization

With a few minor modifications, the CL circuit in Fig. 5 can be used to model CPW series stubs of the type shown in Figs. 2 and 3. The four-port impedance matrix is first reduced to two-ports by connecting ports 1 and 2 in series and appropriately terminating port 3 in either an open- or short-circuit (Fig. 6). In addition, discontinuity effects introduced by the transverse slot segments must be considered. The effect of slot segment L_2 is modeled as a shunt capacitance, C_{12}, across the port 1–2 connection. The capacitance of this slot is derived from the inductance (L_{12}) of its physical dual, a strip of length L_2, and width G_1 [17]. As the slot and strip can also be shown to be electrical duals [7], the capacitance and inductance are related by the following:

$$C_{12} = L_{12}\frac{\eta_o^2}{4\epsilon_{re}} \tag{4}$$

where ϵ_{re} is the effective dielectric constant. For the open-end stub, the slot segment L_3 is treated in the same manner, leading to the capacitance C_{30} indicated in Fig. 6.

The quasi-static technique outlined here has demonstrated excellent agreement with a moment-method analysis for a variety of stub dimensions and substrates. In Fig. 7, a comparison of the two methods is shown for the case of a GaAs-supported, CPW open-end stub.

The CL analysis is especially useful in this paper since it allows rapid characterization of stubs with arbitrarily located, integrated MIM capacitors. In order to incorporate a capacitor into the stub model, the CL's are separated at the capacitor location and the appropriate lumped reactance is inserted. The analysis is very accurate since the small physical size of the capacitors results in nearly ideal performance over a broad

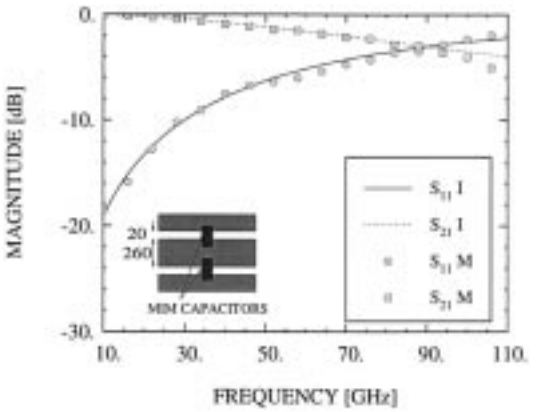

Fig. 8. Measured S-parameters of two 25-fF shunt capacitors on a 67-Ω microshield transmission line (M), compared to an ideal lumped-element equivalent circuit (I).

frequency range. To demonstrate, the measured S-parameters of two 25-fF shunt capacitors in parallel on a 67-Ω microshield line are shown in Fig. 8, and compared with the calculated results for an ideal lumped-element circuit. The capacitor size is typical of that used in this paper.

III. Low-Pass Filter Implementation

This section describes the procedure for utilizing microshield short-end series stubs in the design of compact low-pass filters. The technique relies on the use of integrated MIM capacitors to match an extracted circuit model for the stub with low-pass filter prototypes, such as those found in [18]. The rejection band response of the filter is tuned by using the CL analysis to determine the optimum capacitor position and element (stub) separation. As will be shown, filters designed in this manner can have low insertion loss and second passbands as high as six to seven times the 3-dB frequency.

A. Design Procedure

The initial step in the filter-design process is to derive an equivalent circuit model for the short-end stub, without the MIM capacitors. This is readily accomplished using the scattering parameters determined from the CL analysis, in conjunction with the commercial circuit simulator Libra.[1] The circuit model topology, which is illustrated in Fig. 9, is accurate for stub lengths up to 45°, a condition which holds into the rejection band for all filters examined herein. More complete models for this stub geometry have been proposed which are accurate beyond the 90° band-stop resonance (e.g., [9]). The model applied here, however, is well-suited for the chosen design approach.

Using the equivalent circuit, a geometry consisting of cascaded series stubs and shunt MIM capacitors is then matched to a selected low-pass filter prototype. For a five-section filter, the layout consists of four stubs arranged in series, with the second and fourth stubs reversed; the equivalent circuit for the entire filter is shown in Fig. 10. From this layout, the five-elements enclosed by dotted lines are defined by neglecting

[1]Libra is a product of the Hewlett-Packard Company.

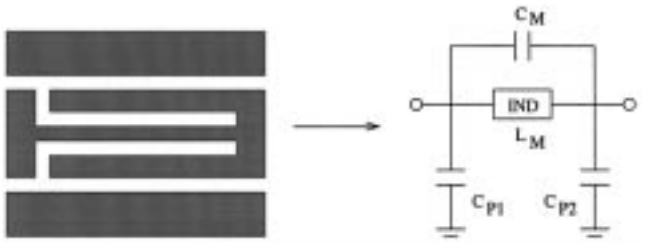

Fig. 9. Equivalent circuit model for the series short-end stub.

capacitors C_M and C_{P1}, which are an order of magnitude smaller than C_{P2}. Stub lengths L_{S1}, $L_{S2}+L_{S3}$, and L_{S4} (see Fig. 11) are selected to obtain the required series inductances. These lengths fix the respective values for capacitors C_{P2}, which in turn allows the necessary size of the MIM capacitors to be determined.

The final step in the design process is to optimize the filter response with the aid of the CL analysis. Significant improvement in the stop-band response can be achieved by repositioning the MIM capacitors away from the shorted end of the stubs. Due to the short electrical length of the filter at the lower frequencies, this adjustment has a negligible effect on the passband characteristics. Additional tuning can be achieved by introducing a short length of transmission line between the second and third stubs. This optimization procedure requires minimal computational effort and has proven to be a consistent approach to designing filters with wide rejection bandwidths.

B. Filter Examples

The procedure outlined above has been used to realize five-section microshield low-pass filters, each designed to achieve a 0.02-dB ripple Chebyshev response. The filter dimensions are given in Table I, where the parameters correspond to those illustrated in Figs. 2 and 11.

The first design in Table I serves as a useful baseline to discuss the filter characteristics. For the stated stub geometry, the series inductance (L_M) is about 0.6 nH/mm and the shunt capacitance (C_{P2}) is about 0.044 pF/mm. (Capacitances C_M and C_{P1} are 0.003 and 0.006 pF/mm, respectively). Since the stub length is 700 μm, the inductor elements in Fig. 10 have values of 0.42, 0.84, and 0.42 nH, respectively. Each stub also contributes a capacitance from C_{P2} of 31 fF, which is combined with the overlay capacitors to match the prototype values. As originally presented in [19], the tradeoff between a wide rejection band and minimal out-of-band spurious response is optimized with the MIM capacitors positioned at $L_c = 520$ μm. A 40-μm inter-stub spacing (L_g) is used between all stubs in this design.

A comparison between measured data for filter 1 and the results from the CL analysis is presented in Fig. 12. The measurements were taken in three separate bands up to 117 GHz, but the span from 60 to 70 GHz could not be covered. The measured passband S_{21} varies between -0.2 dB and -0.5 dB from 2 to 20 GHz, and the second passband does not occur until 125 GHz. A comparable stepped-impedance implementation exhibits a (theoretical) maximum rejection of approximately 30 dB and a second passband near 82 GHz [3].

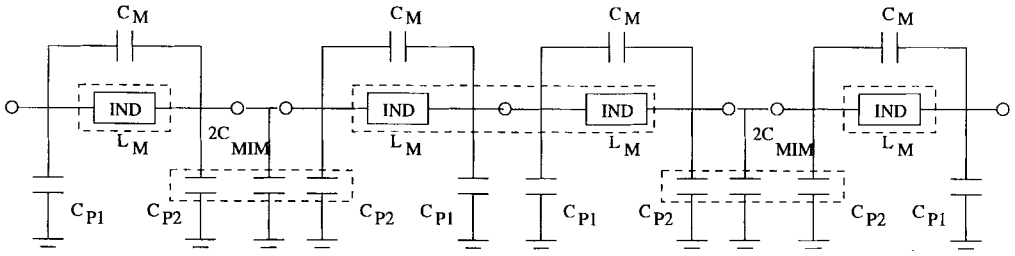

Fig. 10. Equivalent circuit model for the five-section low-pass filter (each section is enclosed in a box). C_M and C_{P1} are neglected in designing the filter.

TABLE I
PARAMETERS FOR FIVE-ELEMENT MICROSHIELD LOW-PASS FILTERS, BASED ON THE GEOMETRIES SHOWN IN FIGS. 2 AND 11. ALL STUB LENGTHS ($L_{s,i}$) AND CAPACITOR LOCATIONS ($L_{c,i}$) ARE EQUAL, AND THE METAL THICKNESS IS 1.0 μM. ALL DIMENSIONS IN THIS TABLE ARE GIVEN IN μM

Design	S_1	S_2	W_1	W_2	G_1	L_s	L_c	L_{g1}	L_{g2}	L_{g3}	C_{M1M}
1	260	50	20	50	20	700	520	40	40	40	42 fF
2	260	20	20	95	20	820	590	40	120	40	76 fF

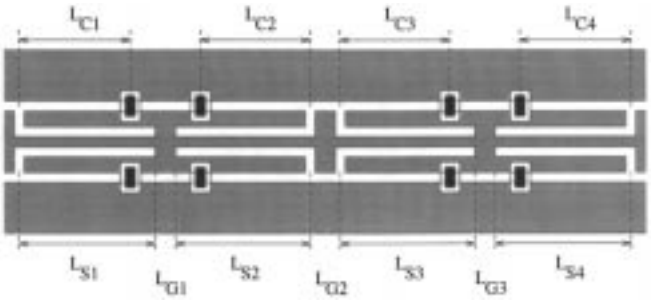

Fig. 11. Metallization pattern for the microshield five-section lumped-element low-pass filter.

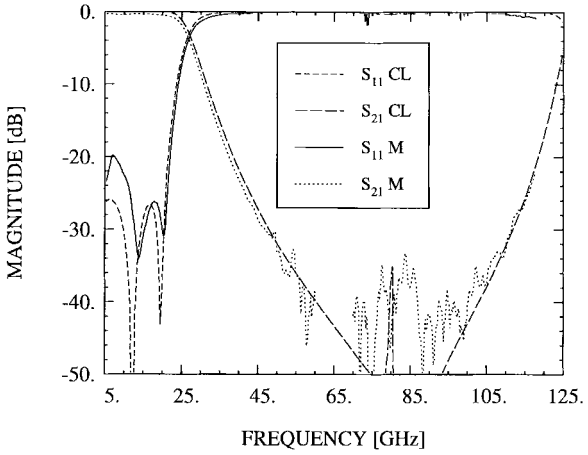

Fig. 12. Measured and predicted performance for a five-section microshield low-pass filter (filter 1 in Table I).

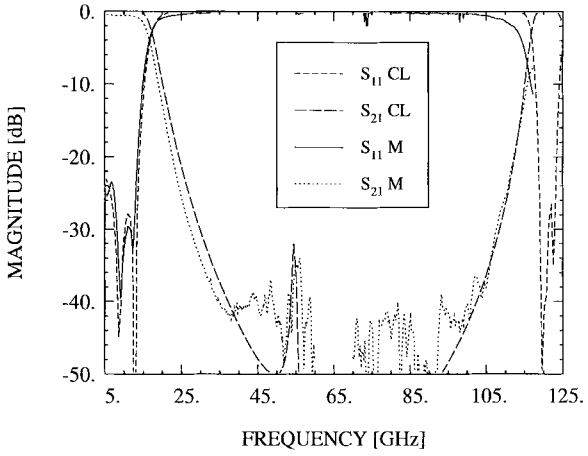

Fig. 13. Measured and predicted performance for a five-section microshield low-pass filter (filter 2 in Table I).

The performance of filter 1 was slightly suboptimal since the fabricated capacitors were 6% larger than the design value, resulting in the predicted spurious response near 80 GHz. The additional structure in the measured data may result from inter-element coupling, which is not accounted for in the CL analysis.

By increasing the per unit length inductance of the stub, the required resonator lengths can be reduced and the width of the rejection band increased. In a modified geometry, the slot width W_2 was widened from 50 to 95 μm with respect to the first design, resulting in a value for L_M of around 0.8 nH/mm. Accordingly, the stub lengths required to realize a given inductance decreased by 25%. The new geometry also provides for wider rejection bandwidths, since the second passband is directly related to the stub lengths.

A second filter design, based on the new stub geometry, is detailed in Table I. In order to capture both passbands in the measured data, the 3-dB frequency was scaled down to 16 GHz. From the measured and predicted responses illustrated in Fig. 13, it is seen that the second passband does not occur until 115 GHz. The measured S_{21} varies between -0.35 and -0.65 dB from 2 to 12 GHz. As with the first results, the low-level spurious response near 55 GHz resulted from the fabricated capacitors being 6% larger than the design value.

Using the CL analysis, a variation of the filter topology illustrated in Fig. 10 was investigated in which three shunt MIM capacitors and two series inductors were employed. In comparison to filter 1, this led to a 63% reduction in the overall filter length. The disadvantage of this implementation is that the individual stub lengths needed to be longer in order to match the prototype element values, which caused the second passband to occur at a lower frequency (100 GHz compared to 125 GHz). Depending on the filter specifications, the reduced filter dimensions could prove to be more significant since the rejection band is still reasonably wide.

In summary, the characteristics of the low-pass filters described here compare favorably with alternative filter topologies. On low permittivity substrates, the line lengths

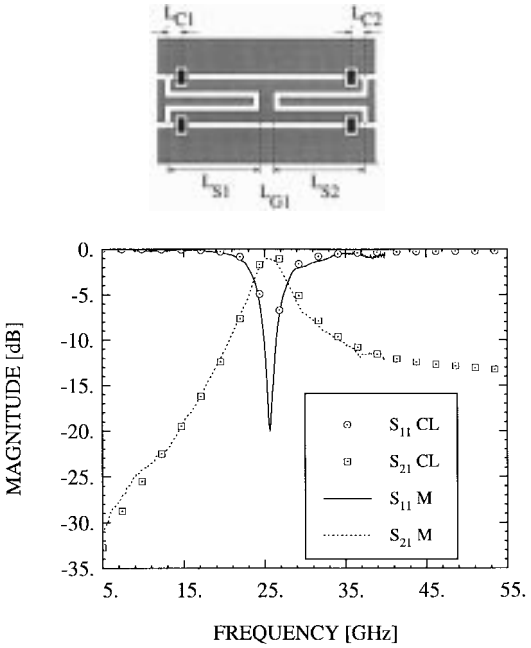

Fig. 14. S-parameters for a narrow-band, microshield bandpass stub (M = measured, CL = CL technique).

in stepped-impedance filters are relatively long and the low impedance sections are wide. Furthermore, an accurate design for mm-wave frequencies requires a rigorous characterization of the parasitics at the impedance steps [4]. These problems are addressed in a design that utilizes shunt open-circuit stubs [20]; however, the shunt stubs result in wide circuit dimensions. In comparison, when using the series stub and MIM capacitor approach, low impedance lines are not required, discontinuities are minimized, and the resulting geometries are compact in both dimensions. For example, the lengths of the filters presented in Table I are comparable to what would result from a GaAs-based stepped-impedance design, although the wide rejection bandwidths will not be obtained using the latter approach.

IV. Bandpass Filter Implementation

The technique of integrating MIM capacitors with series open-end stubs has also been pursued. By itself, the stub exhibits a broad passband resonance (70–100% bandwidth) when the length is approximately $\lambda/4$; these attributes make it useful for dc blocking [21] and in various filter implementations (e.g., [22]). However, the broad bandwidth precludes the use of a single stub in blocking signals near the center frequency. Multiple element configurations may thus be required, and these can occupy considerable circuit area on a low permittivity substrate. It will be demonstrated in the following sections that a solution to the bandwidth problem is achieved using the MIM capacitors.

A. Narrow-Band Bandpass Stub

A narrow-band equivalent of the standard open-end series stub is realized by combining two stubs with MIM capacitors in series (Fig. 14). This configuration exhibits a bandpass response when the total circuit length is approximately $\lambda/4$, with 3-dB bandwidths ranging from around 10% to 30%. For a given stub geometry and capacitor size, the lowest resonant frequency occurs when the capacitors are positioned near the transverse slot L_2 (i.e., L_c is approximately zero).

TABLE II
Parameters for Two- and Three-Section Microshield Band-Pass Filters, Based on the Geometries Shown in Figs. 3, 15, and 16. All Stub Lengths ($L_{s,i}$) Capacitor Locations ($L_{c,i}$), and Stub Separations ($L_{g,i}$) Are Equal, and the Metal Thickness Is 1.0 μm. the Dimensions in the Table Are Given in μm

Design	Sections	S_1	S_2	W_1	W_2	G_1	G_2	L_s	L_c	L_g	C_{MIM}
1	2	260	40	70	65	20	20	1190	40	40	36 fF
2	3	260	40	70	25	20	20	890	40	40	50 fF

The performance of a narrow-band stub that is 80° long (2.6 mm) at the center frequency is shown in Fig. 14. Included in this figure are measured data and the response predicted by the CL analysis. The stub has an 18% bandwidth, 1-dB insertion loss at 25.5 GHz, and 30-dB rejection at 5 GHz. In comparison, a comparable 90° (2.9 mm) open-end series without capacitors was characterized and found to have 0.25-dB insertion loss, but less than 6-dB rejection at 5 GHz.

B. Filter Demonstrations

The single-element stub configuration illustrated in Fig. 14 can be used in multiple-section filters to achieve narrower bandwidths and greater out-of-band rejection. Unlike the short-end stubs, the equivalent circuit model derived for the open-end stub with MIM capacitors does not easily lend itself to a closed-form design approach. However, the characteristics of a single back-to-back stub element can be used to estimate the center frequency, bandwidth, and out-of-band rejection. The filter response can then be tuned by making small adjustments in the stub lengths and MIM capacitor values, with the aid of the CL analysis.

Two examples of filters which have been designed using this approach are described in Table II. In each case, the layout consists of identical single-element stubs (Fig. 14) which are cascaded in series and separated by 40 μm. The two-section design has a center frequency of 31 GHz, a 10% bandwidth, and a midband insertion loss of 1.5 dB (Fig. 15). The three-section design has a center frequency of 31.5 GHz, a 10.5% bandwidth, and an insertion loss of 2.2 dB (Fig. 16). The overall lengths of filters 1 and 2 are 4.9 and 5.6 mm, respectively. Both filters have a second passband at approximately $2f_o$, which corresponds to the quarter-wavelength resonance of an individual open-end stub without the MIM capacitors. The discrepancy in the out-of-band rejection seen in the plots is believed to be due to calibration error and inter-element coupling which cannot be accounted for in the analysis. The effects were characteristic of measurements taken on several filter designs.

V. Conclusion

The design and performance of new topologies for mm-wave low-pass and bandpass filters based on coplanar series stubs with integrated MIM capacitors has been examined. The approach was demonstrated using the micromachined,

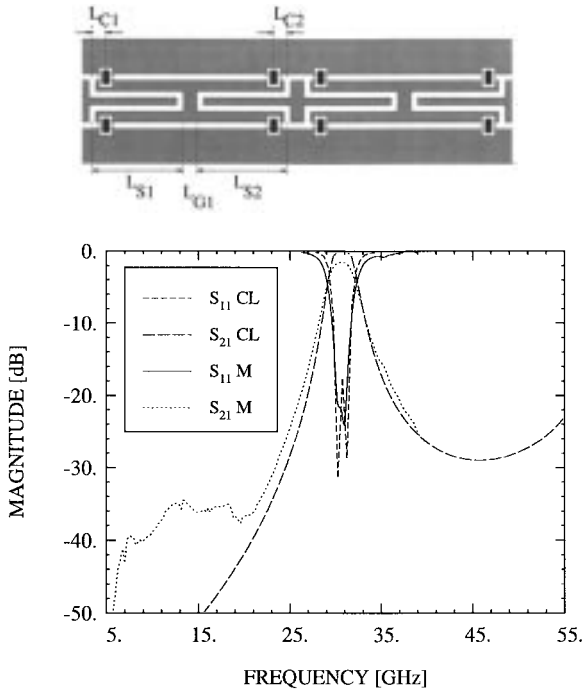

Fig. 15. S-parameters for a microshield two-section bandpass filter (filter 1 in Table II). M = measured, CL = CL technique.

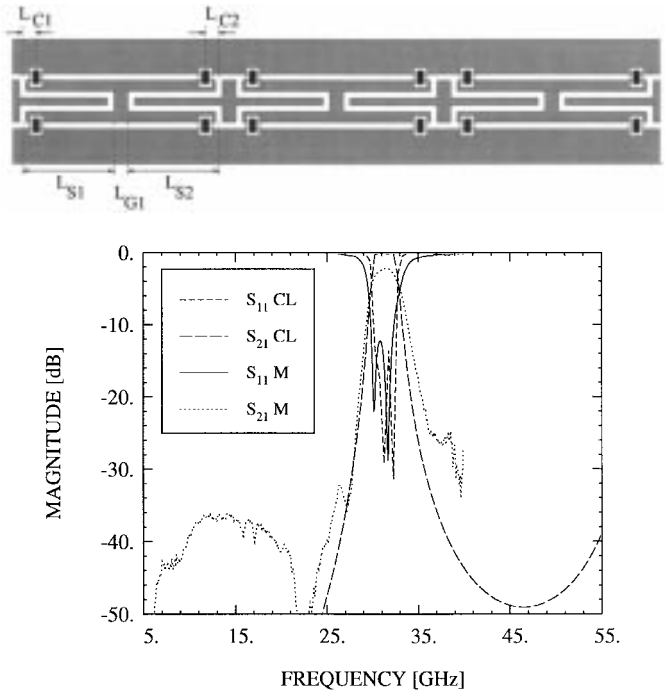

Fig. 16. S-parameters for a microshield three-section bandpass filter (filter 2 in Table II). M = measured, CL = CL technique.

membrane-supported microshield line. A quasi-static, CL analysis provides a fast and accurate approach for the initial filter characterization, as well as the subsequent optimization which is achieved by properly choosing the capacitor placement and the element separation. The lumped-element, low-pass filters which have been realized using this technique have low insertion loss and a second passband which is six to seven times higher than the 3-dB frequency. These characteristics have been verified by measurements taken up to 117 GHz. The topology for the bandpass filters is suitable for bandwidths ranging from 10% to approximately 25%, and as with the low-pass configurations, the designs are compact in both lateral and longitudinal dimensions.

REFERENCES

[1] C. Y. Chi and G. M. Rebeiz, "Planar microwave millimeter-wave lumped elements and coupled-line filters using micro-machining techniques," *IEEE Trans. Microwave Theory Tech.*, vol. 43, pp. 730–738, Apr. 1995.

[2] S. V. Robertson, L. P. B. Katehi, and G. M. Rebeiz, "Micromachined self-packaged W-band bandpass filters," in *1995 IEEE MTT-S Dig.*, Orlando, FL, pp. 1543–1546.

[3] T. M. Weller, L. P. B. Katehi, and G. M. Rebeiz, "High performance microshield line components," *IEEE Trans. Microwave Theory Tech.*, vol. 43, pp. 534–543, Mar. 1995.

[4] S. V. Robertson, L. P. Katehi, and G. M. Rebeiz, "W-band microshield low-pass filters," in *1994 IEEE MTT-S Dig.*, San Diego, CA, pp. 625–628, vol. 2.

[5] T. M. Weller, L. P. B. Katehi, and G. M. Rebeiz, "A 250-GHz microshield bandpass filter," *IEEE Microwave Guided Wave Lett.*, vol. 5, pp. 153–155, May 1995.

[6] E. M. T. Jones and J. T. Bolljahn, "Coupled-strip-transmission-line filters and directional couplers," *IRE Trans. Microwave Theory Tech.*, vol. MTT-4, pp. 75–81, Apr. 1956.

[7] W. J. Getsinger, "Circuit duals on planar transmission media," *1983 IEEE MTT-S Dig.*, Boston, MA, pp. 154–156.

[8] T. Itoh and R. Mittra, "Spectral-domain approach for calculating the dispersion characteristics of microstrip lines," *IEEE Trans. Microwave Theory Tech.*, vol. MTT–19, pp. 30–39, Jan. 1971.

[9] N. I. Dib, L. P. Katehi, G. E. Ponchak, and R. N. Simons, "Theoretical and experimental characterization of coplanar waveguide discontinuities for filter applications," *IEEE Trans. Microwave Theory Tech.*, vol. 39, pp. 873–882, May 1991.

[10] A. K. Rayit and N. J. McEwan, "Coplanar waveguide filters," in *1993 IEEE MTT-S Dig.*, Atlanta, GA, pp. 1317–1320.

[11] F.-L. Lin, C.-W. Chiu, and R.-B. Wu, "Coplanar waveguide bandpass filter—A ribbon-of-brick-wall design," *IEEE Trans. Microwave Theory Tech.*, vol. 43, pp. 1589–1596, July 1995.

[12] D. F. Williams and S. E. Schwarz, "Design and performance of coplanar waveguide bandpass filters," *IEEE Trans. Microwave Theory Tech.*, vol. MTT-31, pp. 558–566, July 1983.

[13] A. K. Sharma and H. Wang, "Experimental models of series and shunt elements in coplanar MMIC's," in *1992 IEEE MTT-S Dig.*, Albuquerque, NM, pp. 1349–1352.

[14] V. K. Tripathi and H. Lee, "Spectral-domain computation of characteristic impedances and multiport parameters of multiple coupled microstrip lines," *IEEE Trans. Microwave Theory Tech.*, vol. 37, pp. 215–221, Jan. 1989.

[15] T. M. Weller, "Micromachined high frequency transmission lines on thin dielectric membranes," Ph.D. dissertation, Dept. of Elect. Eng. and Comput. Sci., Radiation Lab., Univ. of Michigan, Ann Arbor, 1995.

[16] V. K. Tripathi, "Asymmetric coupled transmission lines in an inhomogeneous medium," *IEEE Trans. Microwave Theory Tech.*, vol. MTT-23, pp. 734–739, Sept. 1975.

[17] P. P. Silvester, *Modern Electromagnetic Fields*. Englewood Cliffs, N.J.: Prentice-Hall, 1968, ch. 5.

[18] G. L. Matthaei, L. Young, and E. M. T. Jones, *Microwave Filters, Impedance-Matching Networks, and Coupling Structures*. New York: McGraw-Hill, 1964.

[19] T. M. Weller and L. P. B. Katehi, "A compact millimeter-wave micromachined low-pass filter using lumped elements," in *IEEE MTT-S Dig.*, San Francisco, CA, pp. 631–634, 1996.

[20] S. Kanamaluru, M.-Y. Li, and K. Chang, "Coplanar waveguide low-pass filter using open circuit stubs," *Microwave Opt. Technol. Lett.*, pp. 715–717, Sept. 20, 1993.

[21] P. A. R. Holder, "X-band microwave integrated circuits using slotline and coplanar waveguide," *Radio Electron. Eng.*, vol. 48, no. 1/2, pp. 38–42, Jan./Feb. 1978.

[22] K. Hettak, T. L. Gouguec, J. Ph. Coupez, S. Toutain, S. Meyer, and E. Penard, "Very compact low pass and bandpass filters using uniplanar structures," in *Proc. 1993 EuMC*, Madrid, Spain, pp. 238–239, vol. 1.

Thomas M. Weller (S'92–M'95) received the B.S., M.S. and Ph.D. degrees in electrical engineering from the University of Michigan, Ann Arbor, in 1988, 1991, and 1995, respectively.

He is currently an Assistant Professor in the Electrical Engineering Department, University of South Florida, Tampa. His research involves micromachining applications for microwave and mm-wave circuits, MMIC packaging, electromagnetic modeling, and mm-wave sensors.

Dr. Weller was a co-recipient of the 1996 Microwave Prize from the IEEE Microwave Theory and Techniques Society.

Katherine J. Herrick was born in Rochester, NY, on July 2, 1971. She received the B.S.E. and M.S.E. degrees in electrical engineering from the University of Michigan, Ann Arbor, in 1993 and 1995, respectively, and is currently there pursuing the Ph.D. degree in electrical engineering.

Her research involves development, fabrication, and testing of microwave/millimeter-wave micromachined circuits.

Ms. Herrick is a member of Society of Women Engineers.

Linda P. B. Katehi (S'81–M'84–SM'89–F'95) received the B.S.E.E. degree from the National Technical University of Athens, Greece, in 1977, and the M.S.E.E. and Ph.D. degrees from the University of California, Los Angeles, in 1981 and 1984, respectively.

In 1984 she joined the faculty of the EECS Department, University of Michigan, Ann Arbor. She has authored and coauthored over 260 papers published in refereed journals and symposia proceedings. Her research interests include the development and characterization (theoretical and experimental) of microwave and millimeter-wave printed circuits, the computer-aided design of VLSI interconnects, the development and characterization of micromachined circuits for millimeter-wave and submillimeter-wave applications and the development of low-loss lines for terahertz-frequency applications. She has also theoretically and experimentally studied various types of uniplanar radiating structures for hybrid-monolithic and monolithic oscillator and mixer designs.

Dr. Katehi is a member of IEEE AP-S, MTT-S, Sigma XI, Hybrid Microelectronics, URSI Commission D and a member of IEEE AP-S ADCOM (1992–1995). She is also an associate editor for the IEEE Transactions of AP-S and MTT-S. She has been awarded the IEEE AP-S W. P. King (Best Paper Award for a Young Engineer) in 1984, the IEEE AP-S S. A. Schelkunoff Award (Best Paper Award) in 1985, the NSF Presidential Young Investigator Award and an URSI Young Scientist Fellowship in 1987, the Humboldt Research Award and the University of Michigan Faculty Recognition Award in 1994, and the IEEE MTT-S Microwave Prize in 1996.